Presented at the International Expert Conf. on Measurement and Modeling of Solar Radiation, Edinburgh, 2003

INTERDISCIPLINARY APPLICATIONS OF A VERSATILE SPECTRAL SOLAR IRRADIANCE MODEL: A REVIEW

Christian A. Gueymard
Solar Consulting Services
174 Bluebird Lane
Bailey, CO 80421, USA
Chris@SolarConsultingServices.com

Abstract

A detailed review of different applications that have already been investigated with SMARTS, a versatile spectral solar irradiance model, is proposed here. This review provides examples of applications in many different disciplines, for which recent developments are discussed. Three main types of applications are considered, depending on their spectral range. Purely spectral applications encompass the determination of atmospheric constituents, the performance testing of spectroradiometers, and the development of reference spectra for the rating of photovoltaic or glazing systems, and for standards development in the field of weathering and material degradation. Narrow-band applications include the determination of different UV fluxes and of the UV index, the prediction of illuminance on any horizontal or tilted surface, of the luminous efficacy of direct, diffuse or global radiation, the prediction of the photosynthetically active radiation, and of the irradiance transmitted by different bandpass filters. Finally, some specific broadband applications are reviewed: mesoscale predictions of radiation fluxes, evaluation of circumsolar effects in pyrheliometers, performance assessment of broadband radiation models, and turbidity determination from broadband irradiance data.

1. Introduction

Accurate predictions of incident solar radiation are necessary in many different disciplines, not just solar energy applications. Even though it is relatively easy to evaluate irradiances with appropriate broadband radiation models, *spectral* models provide considerably more flexibility, and possibly more accuracy because of their physical modelling. In many spectrally-dependent applications, they even are the only resource.

A number of spectral radiative codes have been described or used in the literature, and some of them are reviewed elsewhere [1]. However, most of the existing codes are designed to perform specific tasks (e.g., radiative transfer in different layers of the atmosphere) and can hardly be tailored for completely different applications (e.g., predicting the diffuse illuminance on a tilted surface). One of the purposes of the SMARTS code [2-4] is precisely to be as versatile as possible and therefore to address a variety of both spectral and broadband applications, through the use of its different options. More specialized tasks are obviously possible by further manipulating the spectral output of the code.

This paper details many possible applications for which a spectral model can provide the necessary information. The SMARTS code is also used here as an example to discuss some current developments in various disciplines.

2. The SMARTS code

In its earliest derivation [5], the Simple Model of the Atmospheric Radiative Transfer of Sunshine (SMARTS) consisted in an improved version of a Fortran code developed at the Solar Energy Research Institute—now NREL—and usually referred to as SPCTRAL2 [6-10]. SPCTRAL2 has been used in various applications (e.g., [11, 12])—generally related to the solar energy field—but was never updated and thus progressively became outdated. This prompted the development of a completely new model, which evolved from version 2.0 to 2.8, and is described elsewhere [2, 3, 13]. More recently, all calculations related to direct beam irradiance were completely overhauled to improve accuracy and resolution; these important revisions first appeared in version 2.9 released in 2002. Other features were improved or added [4], thereby increasing the code's flexibility. All results discussed in this contribution have been based on versions 2.6 to 2.9.2.

In its latest versions, SMARTS can be used to predict the cloudless direct, diffuse, global, and circumsolar irradiance on any horizontal or tilted surface at 2002 wavelengths from 0.28 to 4 μm. The atmospheric conditions can be selected by the user from a range of default values corresponding to ideal cases (e.g., the U.S. Standard Atmosphere), or can be set to match measured data.

Three types of application are considered in the following sections: (i) those involving spectral irradiance only; (ii) those involving spectral integration of the shortwave spectrum over a limited band; and (iii) those involving broadband irradiance, i.e., after integration over the whole shortwave spectrum.

3. Spectral applications

3.1 Determination of atmospheric constituents

The primary logical use of a spectral model is to predict terrestrial spectra for applications that involve highly spectrally-selective natural phenomena or artificial processes.

Atmospheric extinction caused by molecules and a number of gases and particulates conditions the transfer of solar radiation. Gaseous absorption in particular is highly spectrally-selective. In order to accurately predict terrestrial spectra, radiative transfer models need a precise description of atmospheric conditions, and particularly the columnar amount of the main absorbing gases. However, these amounts can rarely be measured directly. Atmospheric spectral models can then be used advantageously in a reverse way: if spectral radiation is measured over a specific spectral range with sufficient accuracy and resolution, the amount of a variable absorber can be derived. This inverse problem is usually solved with high-resolution atmospheric codes. It has also been successfully approached with SMARTS (or with models that are closely derived from it) to obtain the columnar amounts of atmospheric constituents such as water vapor, ozone, nitrogen dioxide, and aerosols from measured spectra at ground level [14-19]. Because the methodology involved here implies a comparison between modelled spectra and measured spectra that do not have the same resolution, the modelled spectra need to be broadened to match the bandpass shape and width of the monitoring instrument (spectroradiometer or sunphotometer). This can be easily done with the smoothing postprocessor of SMARTS.

Figure 1 shows two different parts of a direct beam spectrum that has been measured with an Optronic OL-750 spectroradiometer at the National Renewable Energy Laboratory (NREL; Golden, CO, latitude 39.74°N, longitude 105.18°W, altitude 1829 m) on 18 October 2002 (a very dry day). It is compared to the output of SMARTS—obtained to match the instrument's 5° field-of-view and smoothed to the 5-nm bandwidth of the OL-750—for the estimated turbidity conditions of that day, and different possible values of precipitable water. The two spectral bands shown in Fig. 1 correspond to moderately strong water vapor absorption. Considering the different sources of uncertainty, good to excellent agreement can be observed between the predicted and measured irradiance. Hence, precipitable water can be estimated by matching the modelled and measured spectra in any one of these bands. In the sample case discussed here, precipitable water is estimated at about 0.4 cm.

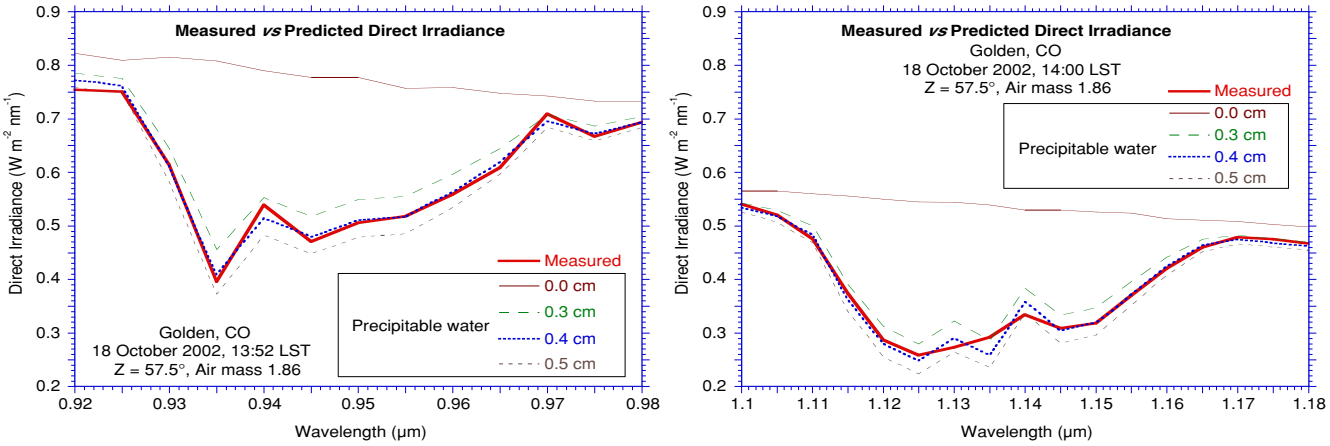

Fig. 1 SMARTS direct normal irradiance predictions for two water vapor absorption bands and four assumed precipitable water values *vs* measured spectrum (thick line) with an OL-750 spectroradiometer in Colorado.

The 940-nm band is the most widely used because it stands within the sensitivity limits of silicon-based detectors. The other band shown in Fig. 1 is only useful if less common instruments can be deployed (e.g., those using a PbS detector, such as the instrument used here). Specific inversion algorithms can be used to retrieve the columnar amount of water vapor (or other constituents) directly, rather than by simple interpolation—even though this is the base case shown in Fig. 1 for demonstration purposes. If the main variables affecting atmospheric extinction (most importantly aerosol optical depth and precipitable water) can be retrieved from spectroradiometric measurements over a limited spectral range (e.g., 400–1000 nm), it is then easy to reconstitute the whole shortwave spectrum with the spectral model. A sophisticated implementation of this method has been described elsewhere [20, 21].

3.2 Performance tests for spectroradiometers

Because of the difficulties and costs associated with the regular characterization, calibration, and maintenance of spectroradiometers, it is possible to use spectral models to test their performance, and possibly detect any malfunction or anomaly. An example of such an approach is provided in Fig. 2, where the OL-750 measurements (from the same experimental dataset as in Fig. 1) are compared to those of a widely used, collocated Li-Cor LI-1800 portable spectroradiometer, and to SMARTS predictions. The percent difference between these spectral predictions (smoothed to match the 5-nm bandwidth of the OL-750

and the 4-nm bandwidth of the LI-1800) and each of the experimental dataset indicates either the apparent error of the model or that of the respective instruments, depending on which reference is trusted most *a priori*.

The only points for which the difference between predictions and OL-750 data is above the instrument's uncertainty (≈4%) are those at 760 nm and 940 nm where sharp absorption lines (for oxygen and water vapor, respectively) exist. They are well documented so that modelling errors should be small there. Therefore, these outliers might indicate a slight wavelength shift of a fraction of nanometer, a frequent problem in this kind of instrument, which results in a sharp local increase in instrumental uncertainty [22]. The same symptom also appears with the LI-1800, but with even more intensity. Furthermore, there is a striking wiggly pattern in the observed percent differences relative to the LI-1800, with sharp transitions at irregularly-spaced wavelengths, $\lambda \approx 450$, 470, 540, 560 and 950 nm. This pattern would be hardly attributed to modelling errors, and furthermore, it has appeared with previous versions of the code and different units of the same instrument [2]. Moreover, this pattern does not appear with laboratory-class instruments such as the OL-750, as evidenced by Fig. 2. This wiggly pattern might result from the rugged design of this portable instrument, considering that its internal mechanisms and filters may have non-negligible mechanical and/or optical tolerances (personal communication with Daryl Myers, 2001). An importance consequence of these findings is that the LI-1800 might not be the most appropriate instrument to accurately derive precipitable water from irradiance measurements at 940 nm, ozone in the Chapppuis band, or spectral aerosol optical depth in the range 400–1100 nm—as is devised in some extrapolation or assessment methods based on this instrument (e.g., [20, 21, 23, 24]).

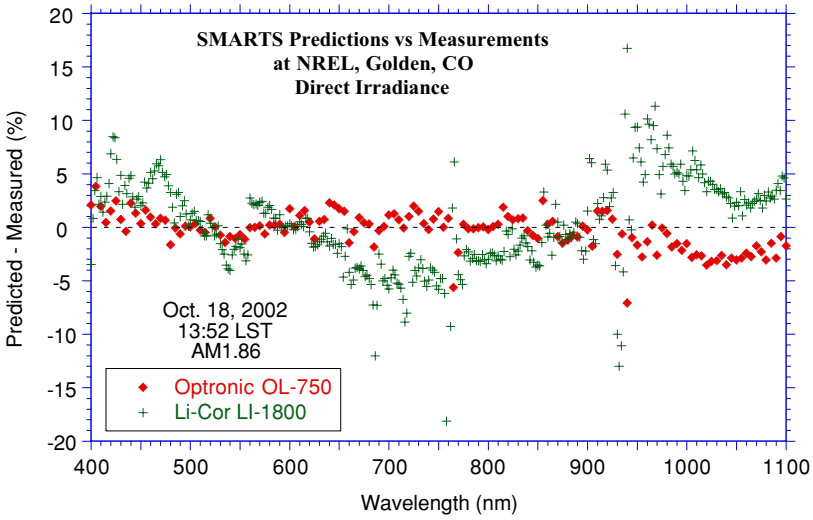

Fig. 2 Percent difference between SMARTS predictions of direct irradiance and measurements of the same by two collocated spectroradiometers in Colorado.

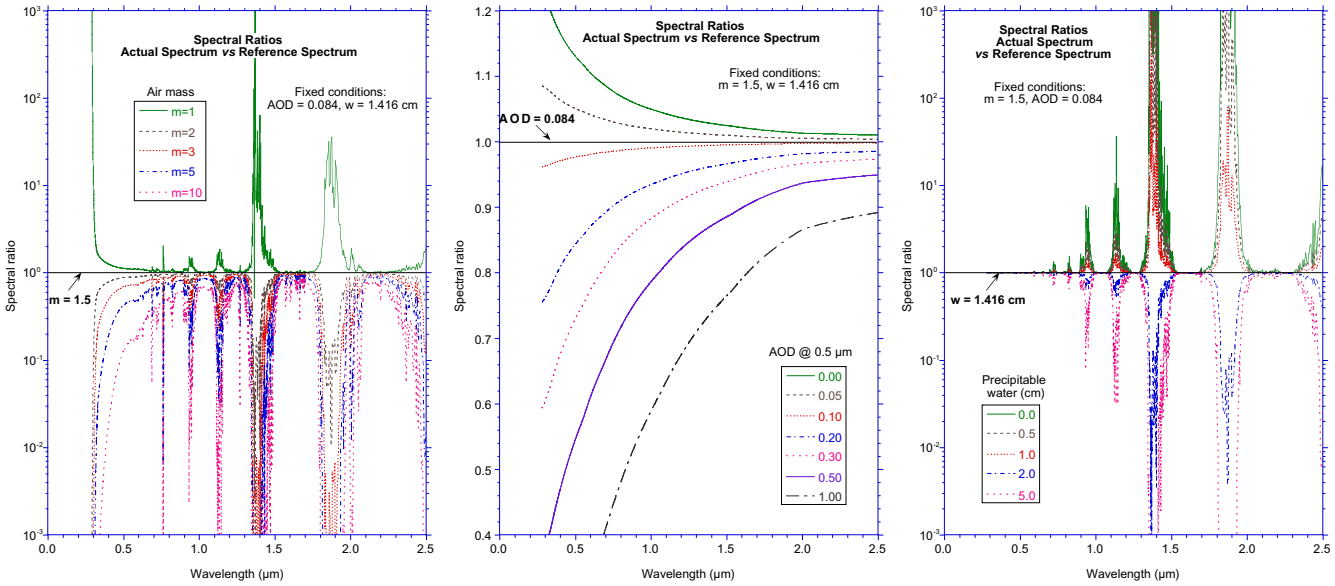

Fig. 3 Spectral variance in direct irradiance (normalized to the reference conditions) caused by variations in air mass (left plot), aerosol optical depth (AOD) at 0.5 μm (center plot), and precipitable water (right plot).

3.3 Reference shortwave spectra

Another important application is the development of reference shortwave spectra tailored for specific spectrally-selective processes. Spectral information is of the utmost importance for some technologies such as photovoltaic (PV) devices and coated glazings. The spectral response of each PV technology being different, the performance of PV cells and systems is known to be dependent on the spectral distribution of the incident solar irradiance in a complex way (see, e.g., [25-34]).

Thus, for testing and rating purposes, the performance of each device needs to be evaluated by direct or indirect reference to a common standard spectrum. For the last two decades, the PV community has been using reference spectra at air mass 1.5 (AM1.5) that have been standardized by the American Society for Testing and Materials (ASTM), the International Electrotechnical Commission (IEC) and the International Organization for Standardization (ISO). A history and critical analysis of these standards is detailed elsewhere [35]. In the last few years, some PV technologies, such as PV concentrators, have experienced considerable development. For this and different other technical reasons [35], it has been argued that the current standards were not completely satisfactory. New reference spectra have thus been prepared with SMARTS [35-37] and are now in the process of being standardized by ASTM. A major difference between the existing standards and the newly proposed standards is that the latter are based on a publicly available and easily implementable code (SMARTS), which is also being proposed as an adjunct standard. This would for instance allow users to consistently evaluate the effect of varied atmospheric conditions on the performance of PV systems by comparison with the standard spectrum, and easily obtain the *spectral mismatch factor* for a particular PV cell [27, 38, 39], or any other spectral correction factor. For instance, Fig. 3 shows the ratio to the newly-proposed reference direct spectrum of three series of direct irradiance spectra obtained when parametrically perturbing the three most important variables under clear sky: air mass, turbidity and precipitable water. This ratioing technique can be generalized: a complex perturbation (resulting from the variation of all three variables combined) can be described by the product of the three fundamental ratios. [Note that only the perturbation caused by turbidity—expressed here by the aerosol optical depth (AOD) at 0.5 μm—is a smooth function of wavelength.] This spectral correction technique cannot be applied to the existing standards because of the lost accessibility to the generating code.

When glazings contribute significantly to the energy balance inside a structure (building or vehicle), solar heat gains must be determined for thermal load and daylighting calculations. Whereas conventional clear glazings are almost spectrally independent, more sophisticated spectrally-selective glazings are now widely used. This complicates transmittance calculations, which must now be performed wavelength-by-wavelength with specialized software (e.g., the WINDOW computer program, http://windows.lbl.gov/software/window/window.html).

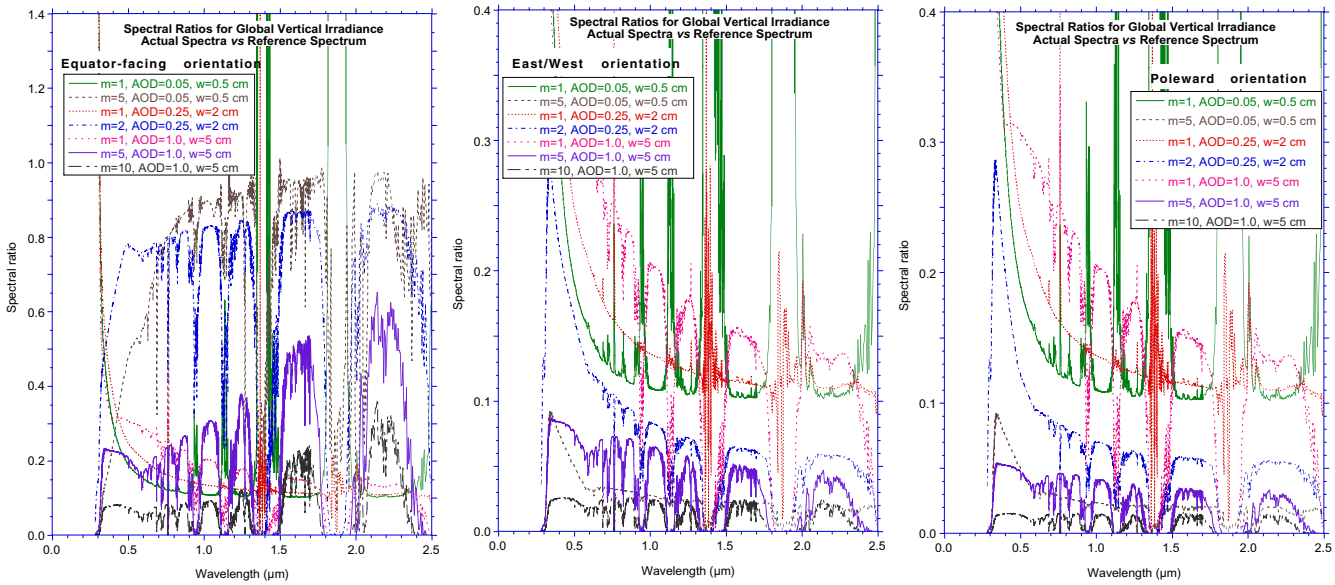

Fig. 4 Spectral ratios between orientation-specific spectra and the 37°-tilt global irradiance reference spectrum for three vertical orientations: equator-facing (left plot), East/West facing (center plot), and poleward (right plot).

As in the case of the PV applications just reviewed, reference spectra are needed to address two complementary problems: first, a single spectrum must be used as a reference so that the performance of all glazings can be compared and rated on the same ideal basis; and second, a variety of spectra is needed to evaluate the optical characteristics of glazings under more realistic conditions, which can be either extreme (for cooling load calculations) or average (e.g., over a period of one year or more to evaluate energy consumptions). In most cases, glazings are installed on *vertical* walls or surfaces. A review of the literature has not revealed the existence of any reference spectrum for vertical surfaces. For rating purposes, the ASTM/ISO AM1.5 global spectrum incident on a 37°-tilted surface is generally used. This spectrum is dominated by the direct beam component because the tilted surface faces the sun at a near-normal incidence. In the real world, windows are directly illuminated by the sun only a fraction of the time—if at all. Defining a *single* reference spectrum for all possible geometries (tilt, azimuth, shading) and realistic atmospheric conditions is thus close to impossible. It is thus suggested that a new reference spectrum be adopted, preferably the same as that for PV applications, and that users be able to derive secondary spectra for each specific application, while remaining consistent with this new reference spectrum.

Figure 4 provides examples of spectral ratios (similar to those in Fig. 3) for vertical walls of different orientations and for different atmospheric conditions and sun positions. The newly-proposed 37°-tilt global spectrum [35] is used here as the reference. The sun's zenith angle is varied but its azimuth is fixed at the local meridian (solar noon). A fixed ground albedo (0.2) is assumed here, and no structural shading or reflection is considered. (Taking all these variables into account would considerably complicate the analysis.) The results in Fig. 4 show dramatic differences in the spectral ratios, depending on atmospheric conditions and window orientation. However, the ratios for the East/West and poleward orientations are almost identical, due to the fact that the sun is not illuminating these surfaces. Hence the corresponding spectra are purely diffuse, explaining also why the spectral ratios for these two orientations are considerably less than 1. It can be also observed that the ratios for the equator-facing orientation are significantly <1 under most circumstances, with large differences in spectral shape. These findings support the recommendation that, for accurate transmittance and solar heat gain calculations with highly spectrally-selective devices, consideration for the actual (site and time dependent) spectral distributions involved is necessary.

3.4 Reference UV spectra

Spectral models are of great help to predict spectra in the ultraviolet (UV) because of the extreme difficulty to obtain accurate spectral ground-based measurements below about 300 nm, due to the weakness of the signal and calibration uncertainties. Predicted UV spectra can be useful in different ways. For instance, they are needed in photobiological studies to study the effect of UV radiation on living organisms. The UV dosage is then obtained by a convolution of the terrestrial spectrum with the action spectrum of the specific biological process under scrutiny. These calculations can be done directly by SMARTS for 14 built-in action spectra. The most important of these action spectra is certainly the CIE erythema spectrum [40], which is used in particular to define the *UV index*—now part of meteorological forecasts. These UV applications are further discussed in Section 4.1.

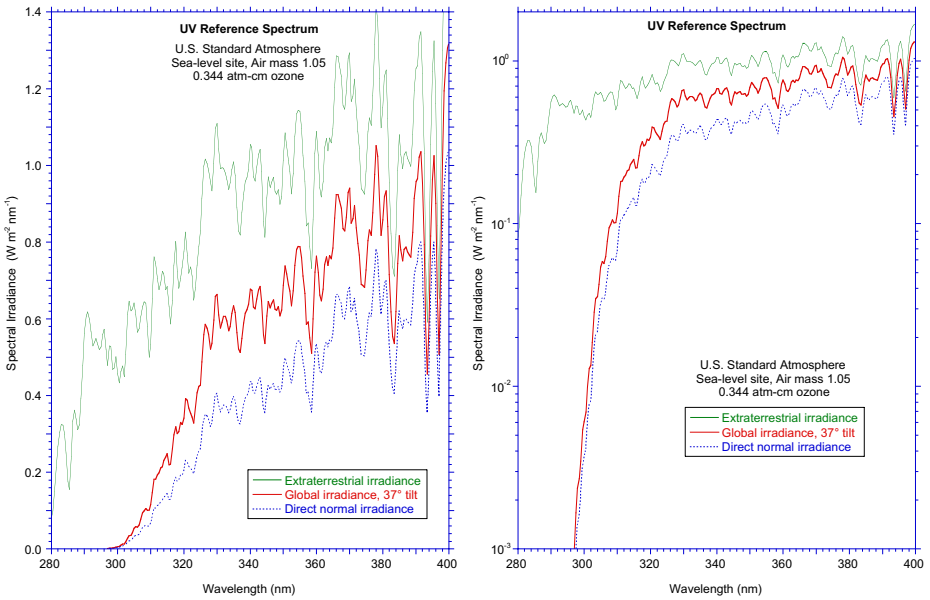

Fig. 5 Proposed reference UV spectra for weathering tests: Global irradiance on a sun-facing 37°-tilt and direct normal irradiance, as obtained by SMARTS. The linear ordinate scale of the left plot is replaced by a log scale in the right plot.

Typical spectra are also necessary to evaluate the weathering and degradation of materials against a common reference. This is particularly important when accelerated weathering procedures are used, which involve exposing samples under favourable atmospheric conditions resulting in "high-UV" irradiance. An existing rule-of-thumb among laboratory weathering testers is that noon summer sunlight offers the appropriate "benchmark" conditions for such tests. It has been observed by different experimentalists at different test sites in the world that, under such clear-sky conditions, the nominal global irradiance at 340 nm is typically 0.68±0.03 W m^{-2} nm^{-1} on a plane normal to the sun's direction (personal communication with Doug Grossman, Q-Panel Lab Products, 2002).

Standardization of these irradiance conditions is now in process at ASTM (personal communications with Daryl Myers and Gene Zerlaut, 2002). Reference "optimal UV" global-tilted and direct normal spectra generated by SMARTS to match these criteria are shown in Fig. 5. The selected conditions are identical to those described earlier for the AM1.5 reference spectra, except for a slightly lower AOD (0.080 at 500 nm) and a much lower air mass (1.05). By comparison with the default extraterrestrial spectrum in SMARTS, the dramatic irradiance decrease in the UV—caused primarily by ozone absorption, but also by Rayleigh scattering and aerosol extinction—clearly appears in Fig. 5.

4. Narrow-band applications

4.1 UV radiation and UV index

There is considerable interest for the effect of UV on living organisms and the environment. Monitoring and predicting UV radiation are now of the utmost importance because of the risk of decreasing protection from the ozone layer. Different kinds of UV measurements and predictions are possible: spectral (as discussed in Section 3.1), UV-A, UV-B, erythemal UV, and total UV. The UV-B and UV-A bands are usually considered to range between 280–315 nm and 315–400 nm, respectively, even though their threshold is sometimes reported as 320 nm (e.g., [41]). The UV-A and UV-B integrated irradiances are readily calculated by SMARTS for both their possible definitions. The erythemal UV is a biological dose-rate that results from the convolution of the UV spectrum with an erythemal action spectrum. The CIE spectrum is usually used for this purpose [40] and a special instrument, known as Robertson-Berger or UV-biometer, provides the means to monitor this important variable. Alternatively, it can be predicted by SMARTS, which also provides the clear-sky UV index (UVI), obtained as the product of the erythemal UV irradiance by 40 m^2 W^{-1}. The predicted UVI for a range of air masses and ozone columnar amounts is shown in Fig. 6. A number of other action spectra are used in photobiology. For instance, the UV-induced damage on plants is frequently associated with the generalized plant damage action spectrum of Caldwell [42]. The dependence of its resulting biological dose-rate on air mass and ozone is also shown in Fig. 6. It can be observed from these plots that the effect of both air mass and ozone is highly non-linear. This implies in particular that these biological effects increase exponentially with a linear decrease in ozone abundance.

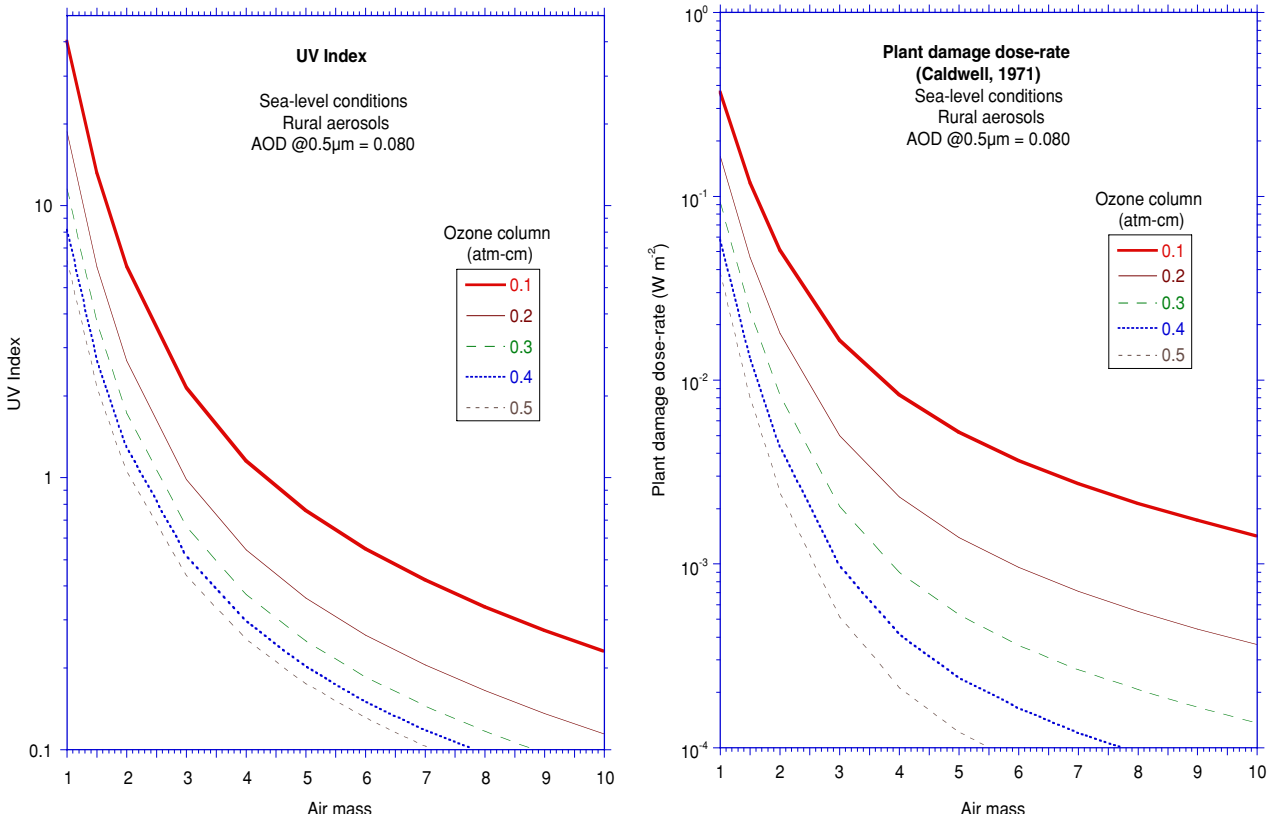

Fig. 6 Typical dependence of UV Index (left plot) and plant damage dose-rate (right plot) on air mass and ozone amount.

Besides air mass and ozone, the erythemal irradiance also depends on other important factors, such as altitude, turbidity, ground albedo, and cloudiness. The relative effects of the first three variables can be explored with SMARTS, to help analyze or complement experimental data obtained in mountainous areas such as the Alps, where altitude and albedo variations are important, and UV doses might reach large values [43].

Because of the low density of the UV radiation monitoring network compared to that of the well-established network of broadband solar radiation, a number of studies have proposed empirical models aimed at predicting the UV-B irradiance or the total UV irradiance from global irradiance, using simple ratios of these quantities. Their relationship can also be analysed parametrically for typical atmospheric conditions, as exemplified in Fig. 7. Whereas the effect of air mass is important, but different, on the two ratios (UV/Global and UVB/Global), the effect of ozone is only important on the UVB/Global ratio. This is easily explained by the fact that UV-A, like global irradiance, is only marginally dependent on ozone, whereas UV-B—only a small fraction of the total UV—is highly dependent on ozone.

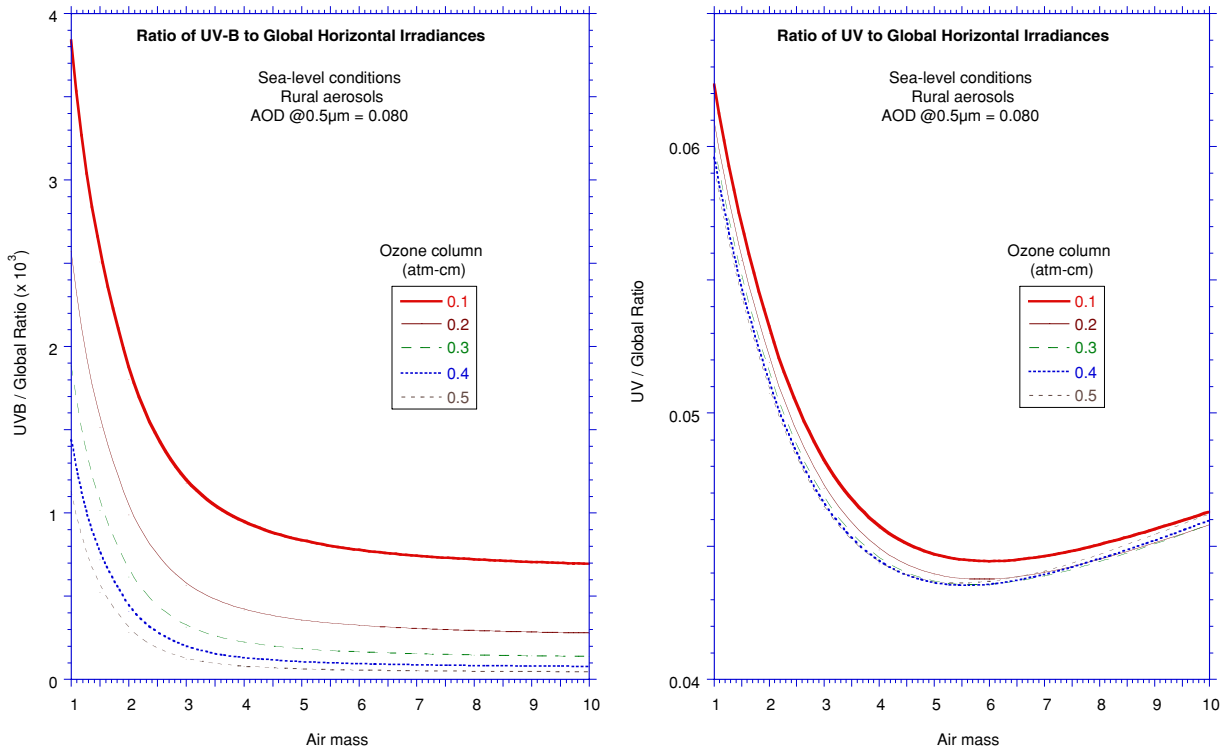

Fig. 7 Ratios of UV-B irradiance (280–315 nm) to global irradiance (280–4000 nm; left plot) and UV irradiance (280–400 nm) to global irradiance (right plot) for typical atmospheric conditions.

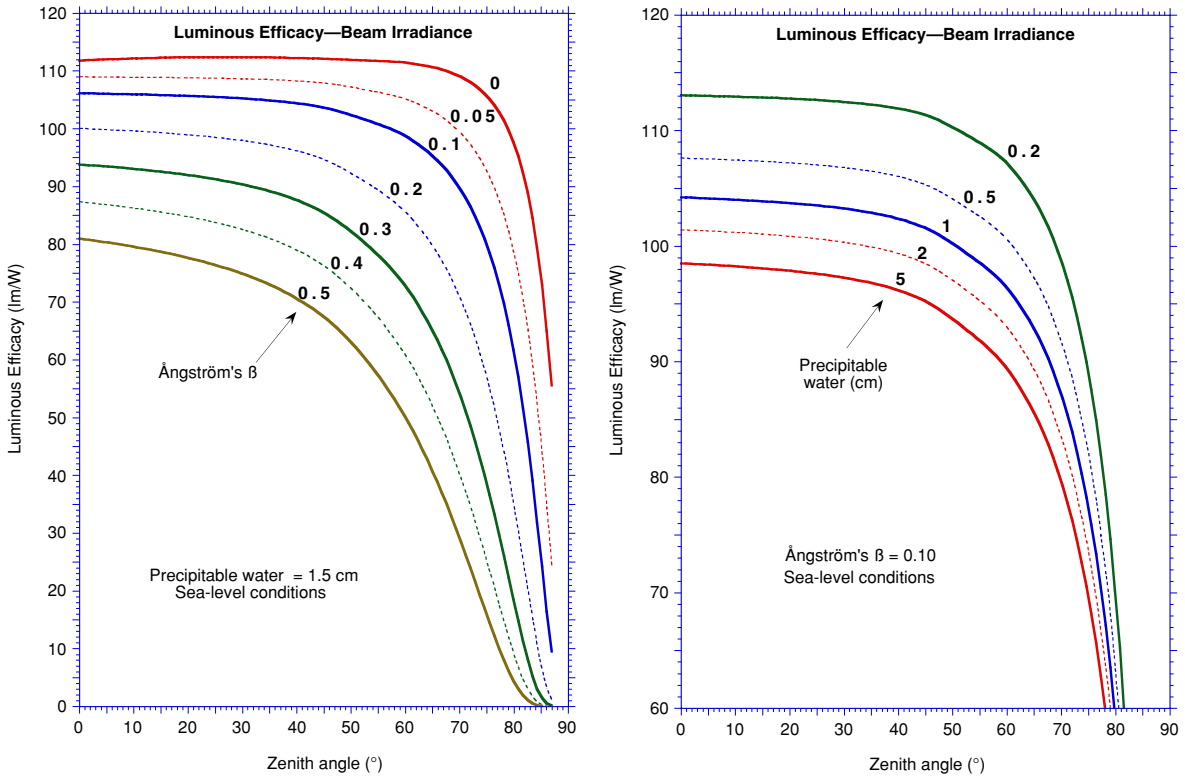

Fig. 8 Luminous efficacy for beam radiation predicted by SMARTS 2.9.2. Left plot: fixed water vapor conditions, variable turbidity; right plot: fixed turbidity, variable precipitable water.

4.2 Illuminance and luminous efficacy

Illuminance and luminous efficacy are important quantities needed in daylighting applications. Most models currently used to determine these quantities are empirically based. In contrast, SMARTS directly provides the direct, diffuse, and global illuminance on any horizontal or tilted surface. Two possible definitions of the photopic curve can be selected to convolute the spectral irradiance: either the CIE 1924 curve, or the more recent CIE 1988 curve. The luminous efficacy of each component (direct, diffuse and global) is also calculated as the ratio between illuminance and the corresponding irradiance. A parametric study, based on version 2.6.3 of SMARTS and the CIE 1924 photopic curve, demonstrated the effect of different atmospheric variables (turbidity, precipitable water, pressure, ozone, and nitrogen dioxide) on the direct, diffuse and global efficacies [44]. Based on the most recent version of the same code and the CIE 1988 curve, Fig. 8 displays the important effect of air mass, turbidity and precipitable water on the direct beam efficacy. Some differences with the previous study are apparent, due to changes in the code and slightly different atmospheric conditions, but the basic features are conserved. More details are provided in a companion paper [45].

Because the effect of aerosols is most concentrated at shorter wavelengths, such as in the visible, it has been argued that the effect of turbidity on illuminance would be best described by a modified turbidity parameter [46]. To this effect, a detailed model aimed at obtaining the illuminance counterparts of the Linke and Unsworth-Monteith broadband turbidity coefficients from common atmospheric variables has been parameterised using reference data provided by SMARTS [47]. This contribution also demonstrated that the illuminance Unsworth-Monteith coefficient has a quasi-spectral behavior and, therefore, that it closely approximates the aerosol optical depth at 555 nm (the peak of the photopic curve). This finding can be used, for example, to obtain climatological information on the aerosol optical depth from the network of stations measuring direct illuminance.

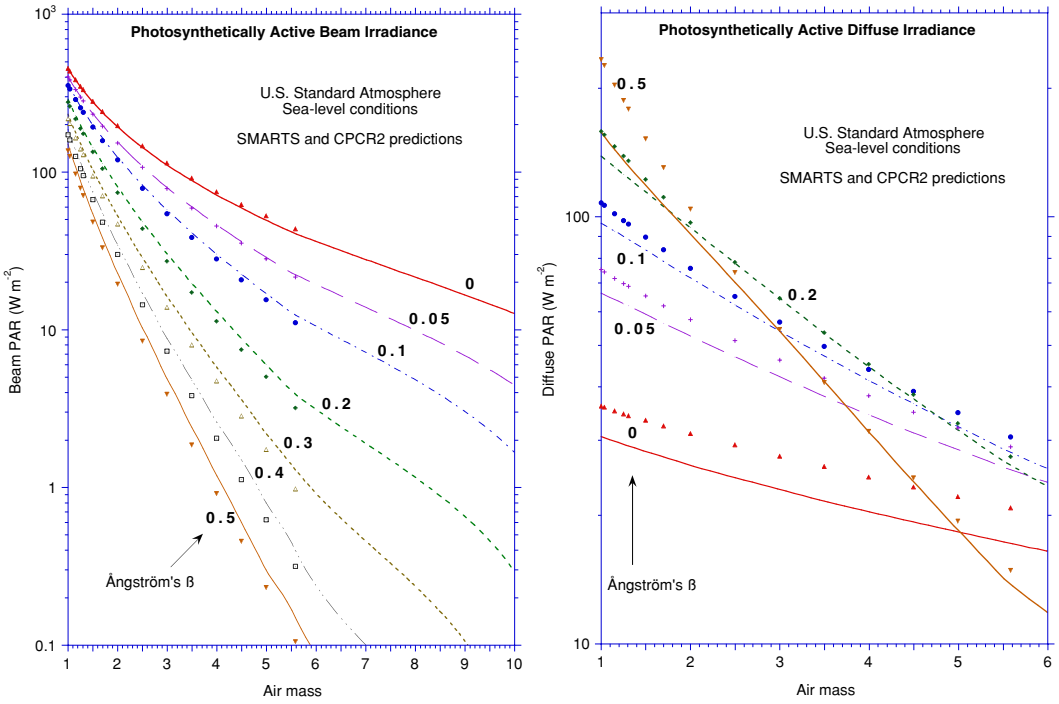

Fig. 9 PAR predictions with CPCR2 and SMARTS as a function of turbidity. Left plot: beam PAR; right plot: diffuse PAR. CPCR2 predictions are represented by symbols and SMARTS predictions by continuous lines.

4.3 Photosynthetically-active radiation

Photosynthetically-active radiation (PAR) is generally defined as the irradiance integrated between 400 and 700 nm. Measurements of PAR are scarce, so that it must be obtained from models most of the time. Like in the case of illuminance, five kinds of calculation methods can be used: models based on remote-sensing data (e.g., [48]), models where PAR is obtained directly from turbidity and other atmospheric conditions [49, 50], simple models where PAR is only a function of broadband irradiance (e.g., [51, 52]), models where PAR is a function of both broadband irradiance and atmospheric variables [53-55], and direct integration of a spectral model's output [56-58]. The latter method is also followed here, using SMARTS to evaluate the beam and diffuse PAR for various ideal turbidity conditions. These are described by an Ångström turbidity coefficient, β, varying from 0 to 0.5, and a wavelength exponent, α, fixed at 1.3. The single-scattering albedo, which seems to have a significant effect on diffuse PAR [49], is fixed here at a constant 0.8 over the whole spectrum. These results appear in Fig. 9, as well as those from a narrow-band model obtained by using the 290–700 nm predictions of the broadband CPCR2 model and correcting them by an air-mass dependent function to obtain PAR, as described elsewhere [54]. The spectral al-

bedo for a canopy of deciduous trees is selected here for the SMARTS simulations, yielding a band-average albedo of about 0.07, value which is used for the CPCR2 simulations. All the other atmospheric conditions are according to the U.S. Standard Atmosphere for a sea-level site.

TABLE 1 Coefficients to calculate PAR from the CPCR2 model and eqn (1).

ß	0.0	0.05	0.10	0.20	0.30	0.40	0.50
Beam PAR							
a_0	0.43084	0.43142	0.43108	0.44268	0.43498	0.44813	0.43865
a_1	0.18304	0.13816	0.09234	-0.051537	-0.04110	-0.086202	-0.093991
a_2	-0.0038417	-0.0067585	-0.0067341	0.0020088	-0.00010831	0.0041378	0.0050001
a_3	0.37119	0.29796	0.21887	-0.0066988	0.039057	0.046462	0.045265
a_4	0.027492	0.028994	0.036335	0.025181	0.057263	0.053435	0.096169
Diffuse PAR							
a_0	.41050	0.36477	0.37846	0.42091	0.42306	0.38557	0.28844
a_1	.40737	0.78864	0.67041	0.22091	0.065074	0.019087	0.073243
a_2	-0.027064	0.0025265	-6.2887E-5	0.0063958	0.0063306	0.0055597	-0.0017321
a_3	0.60922	1.0193	0.76691	0.10131	-0.10985	-0.18894	-0.16277
a_4	-0.040865	0.047891	0.059422	0.061971	0.053868	0.051842	0.051270
Global PAR							
a_0	0.42671	0.42448	0.41741	0.41236	0.39779	0.36976	0.32009
a_1	0.24635	0.14343	0.15145	0.0014725	-0.043876	-0.062844	-0.042271
a_2	0.011884	0.010139	0.0088484	0.0072152	0.0054936	0.0057618	0.0035468
a_3	0.49910	0.26959	0.27238	-0.048827	-0.14992	-0.21272	-0.21199
a_4	0.058099	0.046993	0.047272	0.032247	0.024071	0.025123	0.025974

It appears that both models are in good agreement for beam PAR in all cases. Discrepancies, however, are obvious when comparing the diffuse PAR predictions. In most cases, the CPCR2 predictions are significantly larger than those of SMARTS. These findings are consistent with those in two independent investigations based on experimental data [49, 56]. CPCR2 predictions were found to be good for beam PAR, but too high for diffuse PAR, whereas all SMARTS predictions were found of good accuracy. This indicates that the polynomial functions used to obtain diffuse PAR from CPCR2's beam and global irradiance (see eqns (30) and (31) in [54]) are not appropriate. Using SMARTS as the reference, the PAR/Broadband ratios for beam, diffuse and global radiation—R_b, R_d and R_g, respectively—are more accurately calculated with the following function

$$R_i = \mathrm{PAR}_i / E_{i1} = (a_0 + a_1 m + a_2 m^2)/(1 + a_3 m + a_4 m^2) \quad (1)$$

where i represent subscripts b, d, or g; E_{i1} is the 290–400 nm ("band 1") horizontal component irradiance obtained with CPCR2 for specific atmospheric conditions; m is the optical air mass, and coefficients a_j (j = 0–4) are given in Table 1 for each component (beam, diffuse and global) and discrete values of β. Usual interpolation procedures can be used for other values of β. Equation (1) can be used to predict PAR from CPCR2 with an accuracy comparable to that of SMARTS. As pinpointed in [49], the advantage of using CPCR2 is that, with a single execution of the model, both broadband and PAR fluxes can be generated.

4.4 Filter radiometry

The use of cutoff or bandpass filters in radiometry dates back to the landmark contributions of Ångström (e.g., [59-61]) and Schüepp [62], in particular. In most applications, a set of colored glass filters is mounted on a filter wheel in front of a pyrheliometer to successively measure the incident beam irradiance within specific bands of the spectrum, and derive turbidity information. This technique has been recommended during the International Geophysical Year of 1956 [63], and was subsequently used in a number of turbidity investigations across the globe. A variant of this technique consists in replacing the transparent glass dome of pyranometers by a colored dome to obtain the global or diffuse irradiance within specific bands of the spectrum.

The main advantages of the method are its simplicity, ease of calibration and low cost, especially compared to the more recent spectral technique using multiwavelength sunphotometers, whose first cost and frequent need for delicate calibration at dedicated sites are serious limitations to their widespread use. However, the filter pyrheliometry technique also has limitations of its own. Besides a number of experimental difficulties, the data reduction process developed by Ångström [60] to obtain both β and α, seems to have failed producing repeatable and accurate results. Some experimenters reported considerable scatter in instantaneous values of α, with too frequent, unphysical negative values (e.g., [64, 65]). Others have argued that only extremely accurate pyrheliometric data could provide reasonably meaningful α values, due to exponentially increasing errors along the reduction process (e.g., [60, 66]), or to the parasitic effect of circumsolar radiation [67].

One of the main problems that seems to prevent an accurate determination of α is that, with the widely-used Ångström method, its value is obtained from two closely located spectral bands. Any error in the band irradiances produces consider-

able error in the estimated α. A detailed analysis of the experimental difficulties of such an approach can be found elsewhere [68, 69]. As in multiwavelength sunphotometry, the remedy to this problem might reside in the use of more than three cutoff filters [70], or in a multi-band optimization technique [71]. Furthermore, the use of a spectral radiative code might help improve the outdated calculation method of Ångström [60], while adding the flexibility of taking the circumsolar effect automatically into account. Recent investigations [71, 72] have used SMARTS to perform such calculations. However, it seems that more detailed studies will be necessary before a generalized and accurate method—taking the variations in cutoff wavelength due to temperature effects or other factors, for instance—can become operational under all atmospheric and experimental conditions.

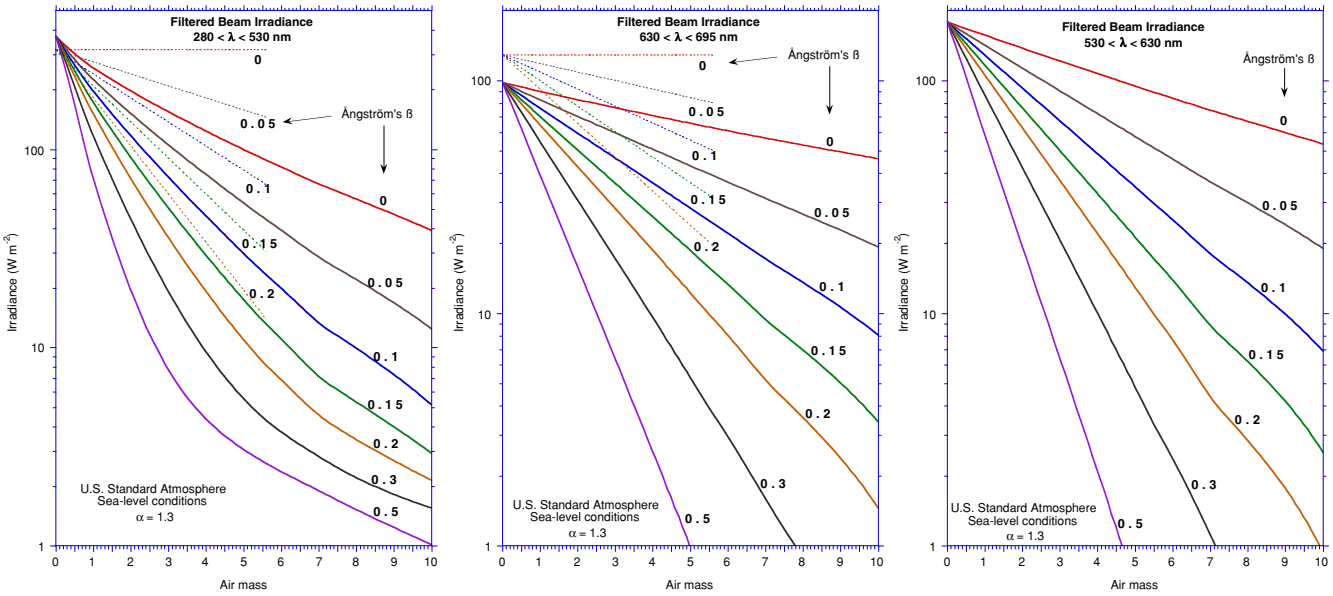

Fig. 10 Predicted irradiances for filtered beam irradiance. Left plot: OG530 filter, λ < 530 nm (K band); center plot: RG630 and RG695 filters, 630 < λ < 695 nm (R band); right plot: OG530 and RG630 filters, 530 < λ < 630 nm (O band). Straight lines: SMARTS predictions; dotted lines: equations by Ångström, 1961 ($m \leq 6$, $\beta \leq 0.2$).

One step in this direction may consist in a reevaluation of the irradiance transmitted by different filter combinations. As an example, version 2.9.2 of SMARTS has been used here to recalculate this quantity for the two basic bands in Ångström's method: the "K" band with λ<530 nm (using the OG530 filter), and the "R" band for 630< λ<695 nm (using the RG630 and RG695 filters in combination). Moreover, similar calculations have been also done for the band obtained when combining the OG530 and RG630 filters, hereafter band "O" for *orange* (530< λ<630 nm). The nominal transmittance data for the three filters involved have been used here, according to the manufacturer's specifications, and the corresponding "filter factors" have been calculated and used to obtain each filter's normalized transmittance. These transmittance curves have been convolved with SMARTS predictions for a U.S. Standard Atmosphere, air masses between 1 and 10, $\alpha = 1.3$, and β varying from 0 to 0.5. These results are plotted in Fig. 10, where they are compared to the application of Ångström's fornulas (that were limited to $m \leq 6$ and $\beta \leq 0.2$ [60]). The following observations can be made from these plots:

- The irradiance in bands R and O nearly perfectly follows an exponential decrease with m, indicating that it approximately follows the Beer-Bouguer-Lambert law for monochromatic radiation.
- Conversely, the irradiance in band K exhibits some curvature, which is particularly evident for large m or β. Therefore, Ångström's statement that a fixed effective wavelength can be used in this band is only approximately true, and only for the limited conditions he envisioned (m<6 and β<0.2). Whenever the choice is possible, it is certainly better to use band O than band K. When used jointly, bands R and O simulate a two-channel sunphotometer.
- Surprisingly, the two Ångström irradiance formulas do not match their accompanying plots (i.e., his Figs. 6a and 6b). These plots look better than the actual results from his formulas so he probably used a too simple derivation for them (an additional attenuation term due to Rayleigh scattering and gaseous absorption seems to be missing). This explains in great part the large difference between Ångström's results and the newer calculations that appear in Fig. 10. The rest of the differences obviously results from progress in modelling the extraterrestrial spectrum and atmospheric extinction, as well as progress in computing power and resolution, and progress in the filter manufacturing process that led to changes in their transmittance.

These findings suggest that a reduction process based on the newer calculations outlined here would provide more accurate results in β and possibly α than those obtained with Ångström's method.

5. Broadband applications

5.1 Circumsolar radiation for pyrheliometers

Circumsolar radiation is highly dependent on air mass, aerosol optical characteristics, and wavelength (being far more pronounced at shorter wavelengths). SMARTS can be used to predict the spectral circumsolar irradiance within the field of view of sunphotometers or spectroradiometers (which measure direct radiation with a collimator tube), or the broadband circumsolar radiation within the field of view of pyrheliometers. The latter application is particularly important when transferring calibration from one type of pyrheliometer to another one with a different geometry, at a site with different atmospheric conditions than at the primary site of Davos, Switzerland. This is where the World Radiometric Reference (WRR) is maintained and calibration transferred to secondary standards during International Pyrheliometric Comparisons (IPC). When two secondary standard instruments with different field of views are calibrated during an IPC and then used to transfer their calibration to field pyrheliometers during a National Pyrheliometer Comparison, they might exhibit a slight disagreement, in the order of 0.1%, due to the circumsolar effect [73].

For more routine applications, the circumsolar contribution for different pyrheliometer geometries and different aerosol submodels has been calculated with SMARTS and parameterised. (see Table 2 and Fig. 8 in [74]).

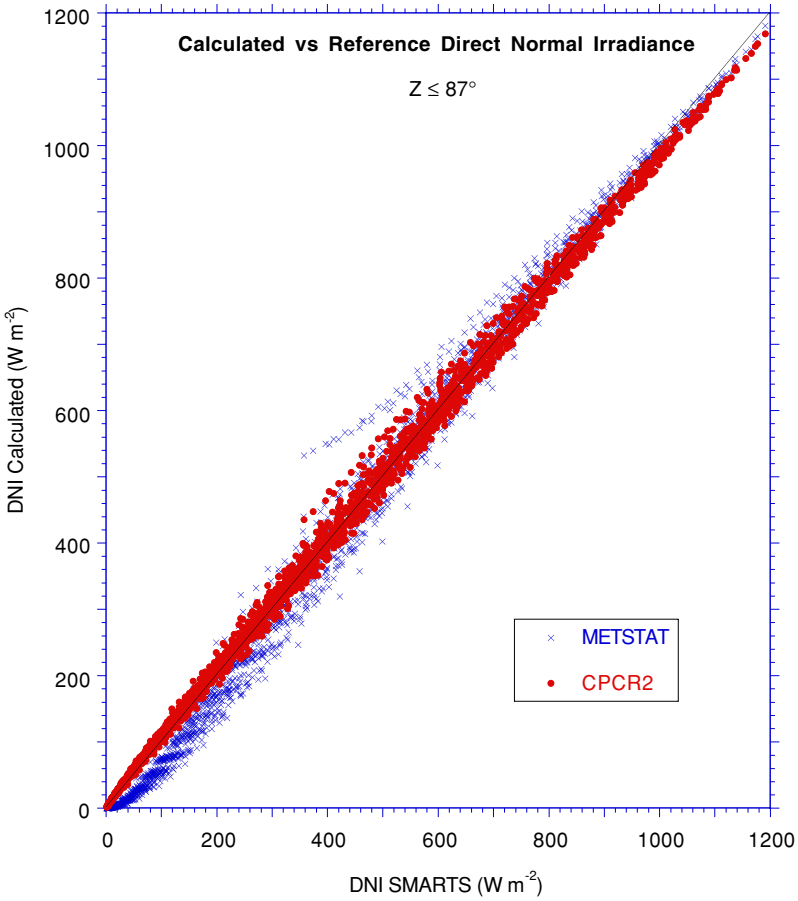

Fig. 11 Scatterplot of DNI predictions by the CPCR2 and METSTAT models *vs* reference predictions by the SMARTS code.

5.2 Performance assessment of broadband radiation models

A number of models have been proposed to evaluate solar radiation from atmospheric variables such as pressure, precipitable water, turbidity, and ozone amount. The performance of these models may be assessed by comparison with benchmark data obtained from either first-class measurements or reference models. Such an approach has been used in [75] to test the accuracy of direct, diffuse, and global irradiance predictions by a few models. More recently [76], the same methodology has been applied to direct normal irradiance (DNI) only, but using more broadband models, as well as reference pyrheliometric and sunphotometric measurements from more sites. A large set of theoretical transmittance and irradiance benchmark data were provided by SMARTS. Figure 11 shows a sample comparison between the DNI predictions of two broadband models, CPCR2 (previously mentioned in Section 3.2.3) and METSTAT [77], and the reference predictions by SMARTS for the whole benchmark dataset (2064 values corresponding to varied solar geometries and atmospheric conditions). CPCR2 demonstrates an excellent behavior under extremely varied atmospheric conditions and is found one of the leading performers in all transmittance and irradiance tests. (Note that it was also the best performer in the earlier study mentioned above [75]).

5.3 Turbidity determination from broadband irradiance data

When turbidity is not measured but direct irradiance data are available, it is possible to derive turbidity from the latter if a direct irradiance model is used in reverse mode. The Linke turbidity factor can thus be directly obtained. However, to obtain the Ångström or Unsworth-Monteith turbidity coefficient, precipitable water must also be accurately known. A number of contributions have been devoted to refine this general technique (e.g., [74, 78-80]). Another technique consists in determining turbidity from an irradiance ratio, such as the diffuse-beam ratio [81] or the diffuse-global ratio [82].

The Linke turbidity coefficient is less informative because it depends not only on aerosol turbidity but also on precipitable water and air mass. Also, contrarily to the Ångström coefficient, it cannot be obtained directly from multiwavelength sunphotometric measurements, which are now available at a large number of sites worldwide [45]. For precise applications, it is therefore preferable to use the Ångström turbidity coefficient. (The Unsworth-Monteith coefficient is also dependent on precipitable water and air mass, but not as much as the Linke factor.) However, the Linke coefficient, T_L, has still a role to play, particularly in climatological studies with an historic perspective. The value of T_L is the solution of the classic equation:

$$E_{bn} = E_{0n} \exp(-m\ \delta_C\ T_L) \quad (2)$$

where, in this case, E_{bn} is the measured DNI, E_{0n} is the extraterrestrial DNI, and δ_C is the optical depth for a clean-dry atmosphere. The precise definition of a clean-dry atmosphere (i.e., an ideal atmosphere without any water vapor or aerosols) has varied over time. Earlier expressions of δ_C [83, 84] did not include any contribution caused by absorption from mixed gases. Moreover, the ozone amount, u_o, was generally fixed at 0.3 atm-cm [85-87]. In a recent contribution [74], δ_C was defined as the sum of the optical depths for Rayleigh scattering, mixed gas absorption, ozone absorption, and stratospheric NO_2 absorption. Version 2.8 of SMARTS was used to obtain a detailed parameterization of δ_C (see eqn (9) in [74]). Using version 2.9.2 of SMARTS and a fixed average stratospheric NO_2 column of 0.2 matm-cm, a simplified parameterization is obtained here as

$$\delta_C = (a_0 + a_1\, m + a_2\, m^2)/(1 + a_3\, m), \quad (3)$$

where m is the *relative* air mass (i.e., non-pressure corrected) and coefficients a_0–a_3 depend on both $q = 1 - p/p_0$ (where p is the site pressure and $p_0 = 1013.25$ mb) and $\eta = u_o - 0.3$:

$$a_0 = \exp(-1.91637 - 0.76596\ q - 0.40062\ q^2) + \eta\ (0.029917 + 0.064295\ \eta)/(1 + 2.6285\ \eta)$$

$$a_1 = \exp(-4.43855 - 0.19482 q + 0.88382\ q^2) - \eta\ (0.00054285 + 0.012383\ \eta)/(1 + 2.4195\ \eta)$$

$$a_2 = -\exp(-8.73026 - 0.082755\ q + 0.77971\ q^2) - \eta\ (0.000039055 - 0.00010991\ \eta)/(1 + 2.2823\ \eta)$$

$$a_3 = \exp(-1.19505 - 0.10653\ q + 1.0114\ q^2) - \eta\ (0.051108 + 0.26936\ \eta)/(1 + 2.5392\ \eta - 0.3236\ \eta^2).$$

[Note that these expressions simplify considerably for a sea-level site ($q = 0$) and a conventional ozone amount, $u_o = 0.3$ atm-cm ($\eta = 0$)].

Results from eqn (3) show notable differences from previous determinations (Fig. 12). By comparison with the previous results in [74] for instance, these differences are the result of a series of modelling changes in version 2.9 of SMARTS, and, more specifically, the consideration of various absorbing trace gases in addition to the uniformly mixed gases. In turn, these changes induce significant changes in the determination of T_L, especially by comparison with the values obtained with the frequently used Kasten's expression for δ_C [84]. For instance, if $m = 2$ and $u_o = 0.5$ atm-cm, these Kasten-based determinations of T_L are about 23% *too high* compared to the results of eqns (2) and (3). Therefore, the comparison of historic T_L datasets to more current determinations must take these changes into consideration to avoid inconsistencies and incorrect climatological interpretations.

When direct irradiance and precipitable water are measured, the Ångström and Unsworth-Monteith turbidity coefficients can be determined accurately using another SMARTS-derived method [74].

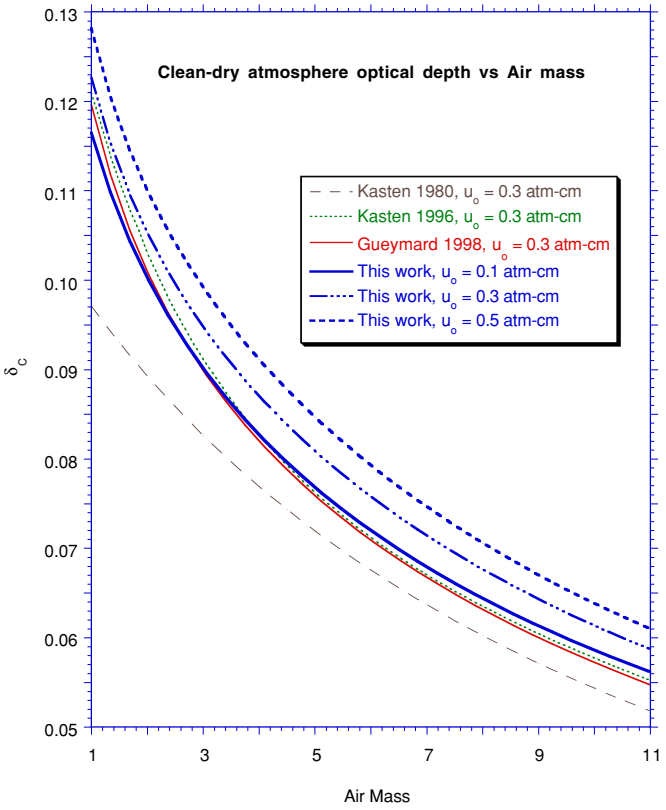

Fig. 12 Various determinations of the clean-dry atmospheric optical depth for a sea-level site, as a function of air mass and ozone amount.

5.4 Mesoscale mapping and predictions of radiation fluxes

An ambitious project aimed at calculating fields of different solar radiation fluxes on a mesoscale grid (22 x 22 km^2) and a hourly time step has been undertaken in Sweden [88]. The targeted area covers Scandinavia, the Baltic countries, and a part of the United Kingdom. The quantities modelled are direct, diffuse and global broadband irradiance, sunshine duration, global PAR, erythemal irradiance and the UV index. SMARTS was used to produce the clear-sky fluxes of these quantities based on estimated atmospheric conditions. For each cell of the grid and each time period, correction functions are used to take cloudiness and ground albedo effects into account. Near real-time predictions are possible using readily available meteorological information. Although such predictions do not have an accuracy comparable to that of ground measurements yet, they show promising results and a lot of potential applications.

6. Conclusion

A versatile spectral radiation model can be a useful tool in many disciplines where solar radiation plays a role. The applications reviewed here constitute a representative sample of typical uses. A rather common denominator between these remarkably different applications is that predictions of terrestrial spectra can advantageously supplement, replace, or even validate the delicate, costly and spectrally-limited measurements of the same. For some parts of the spectrum, such as in the UV below about 300 nm, spectral modelling is the only option.

When comparisons to a reference spectrum are necessary to evaluate the performance of a device (such as a photovoltaic system or a spectrally-selective glazing) under varied atmospheric conditions, the ratioing technique exemplified in Figs. 3 and 4 can be used to simplify the analysis.

Some reference spectra obtained with the latest version of the spectral radiative code discussed here, SMARTS, are in the process of standardization. Therefore, it can be expected that new applications will be developed by the worldwide community of its users.

References

[1] Gueymard, C., *Spectral Models*, in *Solar Energy—The State of the Art*, J. Gordon, ed., James & James Publ., 527-531 (2001).

[2] Gueymard, C., *SMARTS2, Simple Model of the Atmospheric Radiative Transfer of Sunshine: Algorithms and performance assessment*, Rep. FSEC-PF-270-95, Florida Solar Energy Center, Cocoa, FL (1995).

[3] Gueymard, C., Parameterized Transmittance Model for Direct Beam and Circumsolar Spectral Irradiance, *Solar Energy*, **71**, 325-346 (2001).

[4] Gueymard, C., *SMARTS code, version 2.9.2 User's Manual*, Solar Consulting Services (2002).

[5] Gueymard, C., *Development and performance assessment of a clear sky spectral radiation model*, Proc. Solar '93—22nd ASES Conf., Washington, DC, American Solar Energy Society, 433-438 (1993).

[6] Bird, R.E. and R.L. Hulstrom, *A simplified clear sky model for direct and diffuse insolation on horizontal surfaces*, Rep. SERI/TR-642-761, Solar Energy Research Institute, Golden, CO (1981).

[7] Bird, R.E., *A Beer's-law-based, simple spectral model for direct normal and diffuse horizontal irradiance*, Rep. SERI/TR-215-1781, Solar Energy Research Institute, Golden, CO (1982).

[8] Bird, R.E., A simple, solar spectral model for direct-normal and diffuse horizontal irradiance, *Solar Energy*, **32**, 461-471 (1984).

[9] Bird, R.E. and C. Riordan, Simple solar spectral model for direct and diffuse irradiance on horizontal and tilted planes at the Earth's surface for cloudless atmospheres, *J. Clim. Appl. Meteorol.*, **25**, 87-97 (1986).

[10] Riordan, C., Editor ed., *SPCTRAL2, FORTRAN computer program*. NREL, Golden, CO (1990).

[11] Chendo, M.A.C. and A.A.L. Maduekwe, A comparison of spectral irradiance profiles for two Nigerian cities using the SPECTRAL2 computer code, *Renew. Energy*, **3**, 555-558 (1993).

[12] Olseth, J.A. and A. Skartveit, Observed and modelled hourly luminous efficacies under arbitrary cloudiness, *Solar Energy*, **42**, 221-233 (1989).

[13] Gueymard, C., *Updated transmittance functions for use in fast spectral direct beam irradiance models*, Proc. Solar '94 Conf., ASES, San Jose, CA, 355-360 (1994).

[14] Kambezidis, H.D*., et al.*, Radiative transfer. I. Atmospheric transmission monitoring with modeling and ground-based multispectral measurements, *Appl. Opt.*, **36**, 6976-6982 (1997).

[15] Kambezidis, H.D*., et al.*, Radiative transfer. II. Impact of meteorological variables and surface albedo on atmospheric optical properties retrieved from ground-based multispectral measurements, *Appl. Opt.*, **36**, 6983-6988 (1997).

[16] Kambezidis, H.D*., et al.*, *A radiative model based on multispectral direct solar radiation measurements*, Proc. Envirosoft'98, Las Vegas, NV, WIT Press, 89-98 (1998).

[17] Kambezidis, H.D*., et al.*, Case studies of spectral atmospheric transmittance in the ultraviolet and visible regions in Athens, Greece, *Atmos. Res.*, **54**, 223-243 (2000).

[18] Kambezidis, H.D*., et al.*, Total NO_2 column amount over Athens, Greece in 1996-97, *Atmos. Res.*, **57**, 1-8 (2001).

[19] Soule, D.E*., et al.*, *Relation of aerosol optical depth to spectral direct beam solar irradiance for cloudless skies*, Proc. Solar '94, 23rd ASES Annual Conf., San Jose, CA, 402-407 (1994).

[20] Osterwald, C.R*., et al.*, *Extending the spectral range of silicon-based direct beam solar spectral radiometric measurements*, Proc. 20th IEEE Photovoltaic Specialists Conf., 1246-1250 (1988).

[21] Osterwald, C.R. and K.A. Emery, Spectroradiometric sun photometry, *J. Atmos. Ocean. Technol.*, **17**, 1171-1188 (2000).

[22] Myers, D.R., Estimates of uncertainty for measured spectra in the SERI spectral solar radiation data base, *Solar Energy*, **43**, 347-353 (1989).

[23] Cachorro, V.E*., et al.*, A preliminary assessment of a detailed two stream short-wave narrow-band model using spectral radiation measurements, *Solar Energy*, **61**, 265-273 (1997).

[24] Martinez-Lozano, J.A*., et al.*, The parameterisation of the atmospheric aerosol optical depth using the Ångström power law, *Solar Energy*, **63**, 303-311 (1998).

[25] Araki, K. and M. Yamaguchi, Influences of spectrum change to 3-junction concentrator cells, *Solar Energy Materials Solar Cells*, **75**, 707-714 (2003).
[26] Betts, T.R.*, et al.*, *Progress Towards Modelling Solar Spectral Radiation for Optimisation of Amorphous Silicon Photovoltaic Systems*, Proc. Renewable Energy for Maritime and Island Climates, Belfast, (2001).
[27] Emery, K.*, et al.*, *What is the appropriate reference spectrum for characterizing concentrator cells?*, Proc. 29th Photovoltaic Specialists Conf., New Orleans, LA, IEEE, (2002).
[28] Faine, P.*, et al.*, The influence of spectral irradiance variations on the performance of selected single-junction and multi-junction solar cells, *Solar Cells*, **31**, 259-278 (1991).
[29] Gonzalez, M.C. and J.J. Carroll, Solar cells efficiency variations with varying atmospheric conditions, *Solar Energy*, **53**, 395-402 (1994).
[30] Keogh, W. and A. Blakers, *Natural sunlight calibration of silicon solar cells*, Proc. 17th European Photovoltaic Solar Energy Conference and Exhibition, Munich, Germany, (2001).
[31] Meusel, M.*, et al.*, Spectral mismatch correction and spectrometric characterization of monolithic III-V multi-junction solar cells, *Prog. Photovolt. Res. Appl.*, **10**, 243-255 (2002).
[32] Nann, S. and K. Emery, Spectral effects on PV-device rating, *Solar En. Mat. Sol. Cells*, **27**, 189-216 (1992).
[33] Riordan, C. and R. Hulstrom, *Outdoor spectral solar radiation variations and their relationship to photovoltaic device performance*, in *Current topics in photovoltaics, vol. 4*, Academic Press, 1-23 (1990).
[34] Wilson, H.R. and M. Hennies, Energetic relevance of solar spectral radiation on solar cell short circuit current, *Solar Energy*, **42**, 273-279 (1989).
[35] Gueymard, C.*, et al.*, Proposed Reference Irradiance Spectra for Solar Energy Systems Testing, *Solar Energy* (2003, in press).
[36] Myers, D.R.*, et al.*, *Proposed Reference Spectral Irradiance Standards to Improve Photovoltaic Concentrating System Design and Performance Evaluation*, Proc. 29th PVSC, New Orleans, LA, IEEE (2002).
[37] Myers, D.R.*, et al.*, *Revising and validating spectral irradiance reference standards for photovoltaic performance evaluation*, Proc. Solar 2002, Reno, NV, ASME/ASES (2002).
[38] Emery, K.A. and C.R. Osterwald, *Efficiency measurements and other performance-rating methods*, in *Current topics in photovoltaics*, vol. 3, Academic Press, 301-350 (1988).
[39] Seaman, C.H., Calibration of solar cells by the reference cell method—The spectral mismatch problem, *Solar Energy*, **29**, 291-298 (1982).
[40] McKinley, A.F. and B.L. Diffey, A reference action spectrum for ultraviolet induced erythema in human skin, *CIE J.*, **6**, 17-22 (1987).
[41] Kondratyev, K.Y., *Radiation in the atmosphere*, Academic Press (1969).
[42] Caldwell, M.M., *Solar UV irradiation and the growth and development of higher plants*, in *Photophysiology*, A. C. Giese, ed., Academic Press, 131-177 (1971).
[43] Lehmann, A.*, et al.*, *Comparison between models and measurements of direct and diffuse UV erythemal irradiance under clear sky conditions—Analysis of the environmental impacts on the measurements*, Proc. IRS 2000 Conf., Current Problems in Atmospheric Radiation, St. Petersburg, Deepak Publ., (2000).
[44] Gueymard, C., *The effect of cloudless atmospheres on the luminous efficacy of beam, diffuse, and global radiation*, Proc. Solar '95, Minneapolis, MN, American Solar Energy Society, 188-193 (1995).
[45] Gueymard, C., *Importance of atmospheric turbidity and associated uncertainties in solar radiation and luminous efficacy modelling*. This Conference (2003).
[46] Navvab, M.*, et al.*, Analysis of atmospheric turbidity for daylight calculations, *Energy Build.*, **6**, 293-303 (1984).
[47] Gueymard, C. and H.D. Kambezidis, Illuminance turbidity parameters and atmospheric extinction in the visible spectrum, *Q. J. R. Meteorol. Soc.*, **123**, 679-697 (1997).
[48] Li, Z.*, et al.*, Estimation of photosynthetically active radiation absorbed at the surface, *J. Geophys. Res.*, **102D**, 29717-29727 (1997).
[49] Alados-Arboledas, L.*, et al.*, Parametric models to estimate photosynthetically active radiation in Spain, *Agric. For. Meteorol.*, **101**, 187-201 (2000).
[50] Gueymard, C., An atmospheric transmittance model for the calculation of the clear sky beam, diffuse and global photosynthetically active radiation, *Agric. For. Meteorol.*, **45**, 215-229 (1989).
[51] McKree, K.J., A solarimeter for measuring photosynthetically active radiation, *Agric. Meteorol.*, **3**, 353-366 (1966).
[52] Papaioannou, G.*, et al.*, Relationships of photosynthetically-active radiation and shortwave irradiance, *Theor. Appl. Climatol.*, **48**, 23-27 (1993).
[53] Alados, I.*, et al.*, Photosynthetically active radiation: measurements and modelling, *Agric. For. Meteorol.*, **78**, 121-131 (1996).
[54] Gueymard, C., A two-band model for the calculation of clear sky solar irradiance, illuminance, and photosynthetically active radiation at the Earth's surface, *Solar Energy*, **43**, 253-265 (1989).
[55] López, G.*, et al.*, Estimation of hourly global photosynthetically active radiation using artificial neural network models, *Agric. For. Meteorol.*, **107**, 279-291 (2001).

[56] Alados, I., *et al.*, Improved estimation of diffuse photosynthetically active radiation using two spectral models, *Agric. For. Meteorol.*, **111**, 1-12 (2002).
[57] Jacovides, C.P., *et al.*, Urban aerosol and clear skies spectra for global and diffuse photosynthetically active radiation, *Agric. For. Meteorol.*, **87**, 91-104 (1997).
[58] Yang, X. and D.R. Miller, Calculation of potential broadband biologically active and thermal solar radiation above vegetation canopies, *J. Appl. Meteorol.*, **34**, 861-872 (1995).
[59] Ångström, A., On the atmospheric transmission of sun radiation and on dust in the air, *Geogr. Annal.*, **2**, 156-166 (1929).
[60] Ångström, A.K., Techniques of determining the turbidity of the atmosphere, *Tellus*, **13**, 214-223 (1961).
[61] Ångström, A.K. and A.J. Drummond, Basic concepts concerning cut-off glass filters used in radiation measurements, *J. Meteorol.*, **18**, 360-367 (1961).
[62] Schüepp, W., Die Bestimmung der Konponenten der atmosphärischen Trübung aus Aktinometer Messungen, *Arch. Met. Geoph. Biokl.*, **B1**, 257-346 (1949).
[63] CSAGI, *Radiation instruments and measurements*, in *Annals of the International Geophysical Year, Instruction manual, vol. 5, pt. 6*, Pergamon Press, 463 (1957).
[64] Lal, M., On the evaluation of atmospheric turbidity parameters from actinomteric data, *Geofis. Int.*, **12**, 1-11 (1972).
[65] Lal, M., Turbidity parameters for the atmosphere over India, *Tellus*, **29**, 280-281 (1977).
[66] Mani, A., *et al.*, A study of Ångström's turbidity parameters from solar radiation measurements in India, *Tellus*, **21**, 829-843 (1969).
[67] Rangarajan, S., A note on the measurement of atmospheric turbidity, *Tellus*, **25**, 593-594 (1973).
[68] Cachorro, V.E., *et al.*, The influence of Angström parameters on calculated direct solar spectral irradiances at high turbidities, *Solar Energy*, **39**, 399-407 (1987).
[69] Cachorro, V.E., *et al.*, Determination of the Angström turbidity parameters, *Appl. Opt.*, **26**, 3069-3076 (1987).
[70] Vaxelaire, P., *et al.*, Ground-level spectral distribution of solar direct-normal irradiance and marine aerosol attenuation coefficients at Reunion Island, *Solar Energy*, **47**, 189-196 (1991).
[71] Utrillas, M.P., *et al.*, A new method for determining the Ångström turbidity coefficient from broadband filter measurements, *J. Appl. Meteorol.*, **39**, 863-874 (2000).
[72] Tadros, M.T.Y., *et al.*, Determination of Ångström coefficients from spectral aerosol optical depth at two sites in Egypt, *Renew. Energy*, **27**, 621-645 (2002).
[73] Persson, T., *Measurements of solar radiation in Sweden 1983-1998*, Rep. RMK No. 89, Swedish Meteorological and Hydrological Institute (2000).
[74] Gueymard, C., Turbidity determination from broadband irradiance measurements: A detailed multicoefficient approach, *J. Appl. Meteorol.*, **37**, 414-435 (1998).
[75] Gueymard, C., Critical analysis and performance assessment of clear sky solar irradiance models using theoretical and measured data, *Solar Energy*, **51**, 121-138 (1993).
[76] Gueymard, C., Detailed assessment of accuracies achievable in broadband direct transmittance and irradiance predictions with moderate- and high-performance models, Submitted to *Solar Energy* (2002).
[77] Maxwell, E.L., METSTAT—The solar radiation model used in the production of the National Solar Radiation Data Base (NSRDB), *Solar Energy*, **62**, 263-279 (1998).
[78] Grenier, J.C., *et al.*, A spectral model of Linke's turbidity factor and its experimental implications, *Solar Energy*, **52**, 303-314 (1994).
[79] Hay, J.E. and R. Darby, El Chichon—Influence on aerosol optical depth and direct, diffuse and total solar irradiances at Vancouver, B.C., *Atmosphere-Ocean*, **22**, 354-368 (1984).
[80] Louche, A., *et al.*, Determination of Angström's turbidity coefficient from direct total solar irradiance measurements, *Solar Energy*, **38**, 89-96 (1987).
[81] Gueymard, C. and F. Vignola, Determination of atmospheric turbidity from the diffuse-beam irradiance ratio, *Solar Energy*, **63**, 135-146 (1998).
[82] Pinazo, J.M., *et al.*, A new method to determine Ångström's turbidity coefficient: its application to Valencia, *Solar Energy*, **54**, 219-226 (1995).
[83] Feussner, K. and P. Dubois, Trübungsfaktor, precipitable water, Staub, *Gerlands Beitr. Geophys.*, **27**, 132-175 (1930).
[84] Kasten, F., A simple parameterization of the pyrheliometric formula for determining the Linke turbidity factor, *Meteorol. Rdsch.*, **33**, 124-127 (1980).
[85] Grenier, J.C., *et al.*, Atmospheric turbidity analyzed by means of standardized Linke's turbidity factor, *J. Appl. Meteorol.*, **34**, 1449-1458 (1995).
[86] Kasten, F., The Linke turbidity factor based on improved values of the integral Rayleigh optical thickness, *Solar Energy*, **56**, 239-244 (1996).
[87] Louche, A., *et al.*, An analysis of Linke turbidity factor, *Solar Energy*, **37**, 393-396 (1986).
[88] Landelius, T., *et al.*, *A system for modelling solar radiation parameters with mesoscale spatial resolution*, Rep. RMK No. 96, Swedish Meteorological and Hydrological Institute (2001).